

## Enhanced coupled elasto-plastic-damage models to describe concrete behaviour in cyclic laboratory tests: comparison and improvement

I. MARZEC, J. TEJCHMAN

*Faculty of Civil and Environmental Engineering  
Gdańsk University of Technology  
Narutowicza 11/12  
80-233 Gdańsk-Wrzeszcz, Poland  
e-mails: irek@pg.gda.pl, tejchmk@pg.gda.pl*

THE PAPER PRESENTS TWO-DIMENSIONAL FE simulation results of the concrete behaviour under quasi-static cyclic loading using different enhanced coupled elasto-plastic-damage continuum models. Attention is paid to strain localization and stiffness degradation under tensile bending failure. To ensure the mesh-independence, to properly reproduce strain localization and to capture a deterministic size effect, all constitutive models include a characteristic length of micro-structure by means of a non-local theory. Numerical results are compared with corresponding cyclic laboratory tests on concrete specimens under bending. Advantages and disadvantages of coupled models used are outlined. In addition, numerical aspects of implementation and non-local averaging of coupled models are discussed. Finally, a new improved model is proposed to describe strain localization simultaneously under both tension and compression.

**Key words:** beam, concrete, characteristic length, damage mechanics, elasto-plasticity, coupled model, non-local theory, stiffness degradation, stiffness recovery, strain localization.

Copyright © 2012 by IPPT PAN

### 1. Introduction

AN ANALYSIS OF CONCRETE ELEMENTS during cyclic loading under compression, tension and bending is complex mainly due to a stiffness degradation caused by progressive fracture [19, 25, 43, 48]. Fracture is always preceded by formation of a region of strain localization, whose volume is not negligible as compared to specimen dimensions and is large enough to cause significant release and accompanying stress redistribution in the structure [4]. Thus, strain localization is a fundamental phenomenon in concrete under both quasi-static and dynamic conditions and can occur in the form of tensile and shear zones [2]. The determination of the location, width and spacing of localized zones is crucial to evaluate the material strength at peak and in the post-peak regime.

To take into account a reduction of the concrete strength, irreversible (plastic) strains and stiffness degradation, a combination of plasticity and damage theories is physically very appealing since plasticity considers two first properties and damage considers a loss of the material strength and stiffness deterioration. To describe properly strain localization within continuum mechanics, the models should be enhanced in a softening regime by a characteristic length of micro-structure to preserve the well-posedness of the underlying incremental boundary value problem in engineering materials [9]. The presence of a characteristic length allows for considering inhomogeneities triggering strain localization (e.g., size of aggregate) and to describe a size effect (dependence of the strength and other mechanical properties on the size of the specimen) observed experimentally on quasi-brittle and brittle specimens [4, 13].

Within continuum mechanics, plasticity and damage couplings were analyzed with various ideas (e.g., [17, 18, 21, 26, 29, 30, 31, 32, 37, 38, 42, 50, 51, 61]). However, there is still no universal coupled elasto-plastic-damage model for concrete. In addition, the experimental research data on the cyclic concrete behaviour are very poor and limited.

The aim of the paper is two-fold: a) to show the capability of different enhanced coupled elasto-plastic-damage continuum models to describe strain localization and stiffness degradation in notched concrete beams subjected to quasi-static cyclic loading under tensile failure and to discriminate between the performances of each of the models and b) to extend one of coupled elasto-plastic-damage continuum models in order to describe the cyclic behaviour of concrete during both compression and tension. The models were enhanced by a characteristic length of micro-structure connected to non-local averaging of a suitable state variable. Four different concepts of coupled elasto-plastic-damage models were taken into account: by PAMIN and DE BORST [42], CAROL *et al.* [12] and HANSEN and WILLAM [18], MESCHKE *et al.* [38], and finally, the new improved model. In addition, a calibration procedure was shortly discussed.

The first coupled model [42] combines non-local damage with hardening plasticity based on the effective stress and strain equivalence concept [24, 51]. Total strains are equal to strains in an undamaged skeleton between micro-cracks where plastic flow occurs. In the second model [12, 18], plasticity and damage are connected by two loading functions describing the concrete behaviour in compression and tension, respectively. The onset and progression of the material degradation is based upon the strain energy associated with effective stresses and strains. A damage approach (based on second-order tensors) simulates the concrete behaviour under tension, whereas plasticity describes its behaviour under compression. A failure envelope is created by combining a linear Drucker–Prager formulation in compression with a damage formulation in tension based on a conjugate force tensor and pseudo-log damage rate. In turn, in the third

formulation [38], an elasto-plastic criterion in the form of the Rankine criterion with hyperbolic softening is enriched by new components including the stiffness degradation. Following the partitioning concept of strain rates, an additional scalar internal variable is introduced into a constitutive formulation to obtain a split of irreversible strains within plasticity and damage. Based on analysis results of those three formulations, an improved coupled formulation connecting plasticity and damage is presented using a strain equivalence hypothesis following PAMIN and DE BORST [42]. In plasticity, the Drucker–Prager criterion in compression and the Rankine criterion in tension are used [36, 34]. The damage evolution is assumed to be different in tension and compression. The damage in tension and compression includes stress weight factors to take into consideration a stiffness recovery at a crack closure and inelastic strains due to damage.

A characteristic length of micro-structure is included in all models by means of an integral-type non-local approach to investigate strain localization. FE results are directly compared with corresponding quasi-static laboratory tests on notched beams under cyclic bending loading performed by HORDIJK [19] and PERDIKARIS and ROMEO [43].

The innovative points are a) a direct comparison of different variants of enhanced coupled elasto-plastic-damage approaches to study the width of a localized zone and stiffness degradation in concrete beams under tensile loading subjected to cyclic loading, b) improvement of one of coupled models to simulate the cyclic behaviour of concrete in laboratory tests during both tension and compression and c) discussion on numerical aspects of the implementation and non-local averaging of coupled models (detailed implementation algorithms are enclosed in Appendix).

## 2. Local constitutive coupled models for concrete

### 2.1. Model by PAMIN and DE BORST [42]

The first formulation (called throughout the paper model ‘1’) according to PAMIN and DE BORST [42] combines elasto-plasticity with scalar damage assuming that total strains  $\varepsilon_{ij}$  are equal to strains in an undamaged skeleton (called effective strains  $\varepsilon_{ij}^{\text{eff}}$ ). Thus, the plasticity condition is defined in terms of the effective stress:

$$(2.1) \quad \sigma_{ij}^{\text{eff}} = C_{ijkl}^e \varepsilon_{kl},$$

where  $C_{ijkl}^e$  is the linear elastic stiffness tensor (including modulus of elasticity  $E$  and Poisson’s ratio  $\nu$ ) and  $\varepsilon_{kl}$  denotes the strain tensor. The following failure criterion to describe a material response in an elasto-plastic regime is used:

$$(2.2) \quad f_{ep} = F(\sigma_{ij}^{\text{eff}}) - \sigma_y(\kappa_p),$$

wherein  $F$  – the von Mises equivalent deviatoric stress defined in effective stresses  $\sigma_{ij}^{\text{eff}}$ ,  $\sigma_y$  – the yield stress and  $\kappa_p$  – the hardening parameter. Next, the material degradation is calculated with the aid of an isotropic damage model, which describes a progressive loss of the material integrity due to the propagation and coalescence of micro-cracks and micro-voids [24]. This simple isotropic damage continuum model describes the material degradation with the aid of only a single scalar damage parameter  $D$  growing monotonically from zero (undamaged material) to one (completely damaged material). The stress-strain function is represented by the following relationship:

$$(2.3) \quad \sigma_{ij} = (1 - D)\sigma_{ij}^{\text{eff}}.$$

The growth of the damage parameter  $D$  is controlled by a threshold parameter  $\kappa$ , which is defined as a maximum equivalent strain measure  $\tilde{\varepsilon}$  reached during the load history up to time  $t$ ,

$$(2.4) \quad \kappa(t) = \max_{\tau \leq t} \tilde{\varepsilon}(\tau).$$

The damage loading function is described as

$$(2.5) \quad f(\tilde{\varepsilon}, \kappa) = \tilde{\varepsilon} - \max\{\kappa, \kappa_0\},$$

where the parameter  $\kappa_0$  is the initial value of the parameter  $\kappa$  when damage starts. If the loading function  $f$  is negative, damage does not develop. During monotonic loading, the parameter  $\kappa$  grows (it coincides with  $\tilde{\varepsilon}$ ) and during unloading it remains constant. To describe the equivalent strain measure  $\tilde{\varepsilon}$ , a modified definition of the failure criterion by von Mises in terms of strains is used following [44]:

$$(2.6) \quad \tilde{\varepsilon} = \frac{k-1}{2k(1-\nu)} I_1^\varepsilon + \frac{1}{2k} \sqrt{\frac{(k-1)^2}{(1-2\nu)^2} (I_1^\varepsilon)^2 + \frac{12k}{(1-\nu)^2} J_2^\varepsilon},$$

$$(2.7) \quad I_1^\varepsilon = \frac{1}{3} \varepsilon_{kk}, \quad J_2^\varepsilon = \frac{1}{2} \varepsilon_{ij} \varepsilon_{ij} - \frac{1}{6} I_1^{\varepsilon^2},$$

where  $I_1^\varepsilon$  – the first invariant of the strain tensor,  $J_2^\varepsilon$  – the second invariant of the deviatoric strain tensor, and  $k$  – the ratio between the compressive and tensile strength. An exponential softening function by PEERLINGS [44] is chosen to describe the evolution of the damage parameter  $D$ ,

$$(2.8) \quad D = 1 - \frac{\kappa_0}{\kappa} (1 - \alpha + \alpha e^{-\beta(\kappa - \kappa_0)}),$$

wherein  $\alpha$  and  $\beta$  are the material constants. The equivalent strain measure  $\tilde{\varepsilon}$  can be defined in terms of total  $\varepsilon_{ij}$  or elastic strains  $\varepsilon_{ij}^e$ .

The local coupled elasto-plastic-damage model ‘1’ requires the following six material constants to capture the cyclic tensile behaviour:  $E$ ,  $\nu$ ,  $\kappa_0$ ,  $\alpha$ ,  $\beta$ ,  $k$  and one hardening yield stress function. In the case of linear hardening, eight material constants are totally needed (in addition, the initial yield stress  $\sigma_{yt}^0$  at  $\kappa_p = 0$  and hardening plastic modulus  $H_p$ ).

## 2.2. Model by CAROL *et al.* [12] and HANSEN and WILLAM [18]

In the second model (called model ‘2’), a two-surface isotropic damage/plasticity model combining damage mechanics and plasticity in a single formulation is used [12, 18]. A plastic region in compression is described with the aid of a Drucker–Prager criterion. The material experiences in compression permanent deformation under sustained loading with no stiffness reduction. In turn, in tension, damage is formulated in the spirit of plasticity by adopting the concept of a failure condition and a total strain rate decomposition into the elastic strain rate  $d\varepsilon_{ij}^e$  and degrading strain rate  $d\varepsilon_{ij}^d$  (as a result of the decreasing stiffness):

$$(2.9) \quad d\varepsilon_{ij} = d\varepsilon_{ij}^e + d\varepsilon_{ij}^d.$$

The boundary between elastic and progressive damage is governed by the failure function

$$(2.10) \quad f_d = F(\sigma_{ij}, q_d),$$

where  $q_d$  is the history variable describing the evolution of a damage surface. The stress rate is equal to

$$(2.11) \quad d\sigma_{ij} = C_{ijkl}^s(d\varepsilon_{kl} - d\varepsilon_{kl}^d)$$

with  $C_{ijkl}^s$  as the secant stiffness matrix connected with the material damage parameter  $D$  via

$$(2.12) \quad C_{ijkl}^s = (1 - D)C_{ijkl}^e.$$

The application of the secant stiffness is central to the idea that the degraded strains and stresses are reversible, since the material stiffness must degrade to make this idea possible [12, 18]. The degrading strain rate was defined as the excess strain rate beyond the value that corresponded to the stress increment according to the current secant stiffness.

The effective stresses and effective strains are again experienced by the undamaged material between cracks. Assuming the energy equivalence hypothesis, the mutual relationship between the nominal and effective stress and strain is

$$(2.13) \quad \sigma_{ij} = \sqrt{1 - D}\sigma_{ij}^{\text{eff}} \quad \text{and} \quad \varepsilon_{ij}^{\text{eff}} = \sqrt{1 - D}\varepsilon_{ij}$$

and

$$(2.14) \quad \sigma_{ij}^{\text{eff}} \varepsilon_{ij}^{\text{eff}} = \sigma_{ij} \varepsilon_{ij}$$

with

$$(2.15) \quad \sigma_{ij}^{\text{eff}} = C_{ijkl}^e \varepsilon_{kl}^{\text{eff}} \quad \text{and} \quad \sigma_{ij} = (1 - D) C_{ijkl}^e \varepsilon_{kl}.$$

The loading function (Eq. (2.10)) for the Rankine-type damage model is defined in terms of the modified principal tensile conjugate forces:

$$(2.16) \quad f_d = \sum_i^3 (-\hat{y}_{(i)}) - r(L),$$

where  $-\hat{y}_{(i)}$  – the principal components of the tensile conjugate force tensor and  $r(L)$  – the resistance function as the complementary energy. The conjugate force  $-\hat{y}_{(i)}$  is defined with the aid of effective stresses and strains within linear isotropic elasticity:

$$(2.17) \quad -\hat{y}_{(i)} = \frac{1}{2} \langle \sigma_i^{\text{eff}} \rangle \langle \varepsilon_i^{\text{eff}} \rangle,$$

where  $\langle \cdot \rangle$  is the Macauley bracket. Originally, CAROL *et al.* [12] and HANSEN and WILLAM [18] proposed the following resistance function with two parameters  $g_f$  and  $r_0$ :

$$(2.18) \quad r(L) = r_0 e^{-\frac{r_0}{g_f} L},$$

with  $g_f$  – the fracture energy and  $r_0$  – the elastic strain energy at the peak under uniaxial tension,

$$(2.19) \quad r_0 = \frac{(f_t)^2}{2E},$$

where  $f_t$  denotes the tensile strength.

The parameter  $L$  in Eq. (2.16) denotes the pseudo-log damage variable and is calculated with the aid of Eqs. (2.17) and (2.18),

$$(2.20) \quad L = \ln \frac{1}{1 - D}, \quad (D = 1 - e^{-L}),$$

$$(2.21) \quad \dot{L} = \frac{\dot{D}}{1 - D}.$$

However, Eq. (2.18) inadequately describes the post-peak behaviour (i.e., too high sudden stress drop is obtained). As an alternative, a new resistance function with two parameters can be used [35]:

$$(2.22) \quad r(L) = \frac{1}{2} E \kappa_0^2 \exp\left(\frac{L(2-\beta)}{\beta}\right),$$

wherein  $\kappa_0$  denotes the threshold strain value and  $\beta$  is the parameter describing material softening. In addition, the resistance function with three parameters by NGUYEN [39] can be also applied in numerical simulations:

$$(2.23) \quad r(L) = \frac{1}{2} \frac{f_t^2}{E} \left( \frac{E + E_{pt} e^{-L \cdot n_t}}{E e^{-L} + E_{pt} e^{-L \cdot n_t}} \right)^2$$

with  $E_{pt}$  – the damaged stiffness modulus and  $n_t$  – the rate of the stiffness modulus. When simultaneously considering both damage and plasticity, the total strain rate becomes the sum of the elastic, damage and plastic rate:

$$(2.24) \quad d\varepsilon_{ij} = d\varepsilon_{ij}^e + d\varepsilon_{ij}^d + d\varepsilon_{ij}^p.$$

The plastic strains are permanent while the elastic and damage strains are reversible. Therefore, the elastic-damage strain  $d\varepsilon_{ij}^{ed}$  is a part of the total strain:

$$(2.25) \quad d\varepsilon_{ij} = d\varepsilon_{ij}^{ed} + d\varepsilon_{ij}^p.$$

The local coupled elasto-plastic-damage model requires the material constants:  $E$ ,  $\nu$ ,  $\phi$ ,  $\psi$ ,  $g_f$  and  $r_0$  (Eq. (2.18)),  $E$ ,  $\nu$ ,  $\phi$ ,  $\psi$ ,  $\kappa_0$  and  $\beta$  (Eq. (2.22)),  $E$ ,  $\nu$ ,  $\phi$ ,  $\psi$ ,  $f_t$ ,  $E_{pt}$  and  $n_t$  (Eq. (2.23)) and one compressive hardening/softening yield stress function.

### 2.3. Model by MESHKE *et al.* [38]

In the third model (called model ‘3’), an elasto-plastic criterion is enhanced by a component describing the stiffness degradation. The permanent strain rate decomposition is assumed as

$$(2.26) \quad d\varepsilon_{ij}^{pd} = d\varepsilon_{ij}^p + d\varepsilon_{ij}^d.$$

The plastic-damage strain rate  $d\varepsilon_{ij}^{pd}$  is calculated as in classical plasticity. A component associated with degradation and plasticity is obtained by introducing the scalar  $\gamma$ ,

$$(2.27) \quad d\varepsilon_{ij}^p = (1 - \gamma) d\varepsilon_{ij}^{pd} \quad \text{and} \quad d\varepsilon_{ij}^d = \gamma d\varepsilon_{ij}^{pd}.$$

The parameter  $\gamma$  enables one a splitting of effects connected with plastic strains and material deterioration that contribute to an increase of the compliance tensor. The evolution law for the compliance tensor compatible with general form of loading function  $f$  is ( $d\lambda$  – the proportionality factor)

$$(2.28) \quad \dot{D}_{ijkl} = \gamma d\lambda \frac{\frac{\partial f}{\partial \sigma_{ij}} \left( \frac{\partial f}{\partial \sigma_{kl}} \right)^T}{M} \quad \text{with} \quad M = \left( \frac{\partial f}{\partial \sigma_{ij}} \right)^T \sigma_{ij}.$$

The stresses are updated analogously to the standard plasticity theory. To simulate concrete softening in tension, a hyperbolic softening law is adopted,

$$(2.29) \quad \sigma_t(\kappa) = \frac{f_t}{\left(1 + \frac{\kappa}{\kappa_0}\right)^2},$$

where  $\kappa_0$  – the parameter adjusted to the fracture energy.

This local coupled elasto-plastic-damage model requires in tension five constants only, such as  $E$ ,  $\nu$ ,  $f_t$ ,  $\kappa_0$  and  $\gamma$ .

#### 2.4. Improved model

In order to describe the cyclic concrete behaviour under both tension and compression, an improved coupled model (called model ‘4’) was proposed based on the model ‘1’ by PAMIN and DE BORST [42] (which combines elasto-plasticity with a scalar damage assuming a strain equivalence hypothesis). The elasto-plastic deformation is defined in terms of effective stresses according to Eq. (2.1). Two criteria are used in an elasto-plastic regime [36, 34]: the Drucker–Prager criterion with a non-associated flow rule in compression, and the Rankine criterion with an associated flow rule in tension defined by effective stresses (Eq. (2.2)). The yield surface based on the linear Drucker-Prager criterion was assumed in the following form:

$$(2.30) \quad f_1 = q + p \tan \varphi - \left(1 - \frac{1}{3} \tan \varphi\right) \sigma_{yc}(\kappa_1),$$

where  $q$  – the Mises equivalent deviatoric stress and  $p$  – the mean stress. The material hardening/softening is defined by the uniaxial compression stress  $\sigma_{yc}(\kappa_1)$ , wherein  $\kappa_1$  is the hardening-softening parameter. The linear Drucker–Prager criterion is certainly not suitable in a compression regime if a large range of stress is concerned, because it is not able to correctly describe a pressure sensitivity of concrete materials (a curved criterion should be used). For our numerical analysis, where a low pressure level dominates, the adopted simplified criterion is

sufficient. Moreover, this criterion (Eq. (2.30)) is not directly responsible for the failure mechanism when using coupled models. The flow potential is

$$(2.31) \quad g_1 = q + p \tan \psi$$

with  $\psi \neq \varphi$ . In turn, in the tensile regime, the Rankine criterion is used including a yield function  $f_2$  with isotropic softening defined as

$$(2.32) \quad f_2 = \max\{\sigma_1, \sigma_2, \sigma_3\} - \sigma_{yt}(\kappa_2),$$

where  $\sigma_i$  – the principal stresses,  $\sigma_{yt}$  – the tensile stress and  $\kappa_2$  – the softening parameter. The material degradation is calculated within damage mechanics, independently in tension and compression using one equivalent strain measure  $\tilde{\varepsilon}$  proposed by MAZARS [37] ( $\varepsilon_i$  – principal strains):

$$(2.33) \quad \tilde{\varepsilon} = \sqrt{\sum_i \langle \varepsilon_i \rangle^2}.$$

In tension, the same damage evolution function by PEERLINGS [44] as in the model ‘1’ is chosen (Eq. (2.8)). In turn, in compression, the definition by [15] is adopted:

$$(2.34) \quad D_c = 1 - \left(1 - \frac{\kappa_0}{\kappa}\right) \left(0.01 \frac{\kappa_0}{\kappa}\right)^{\eta_1} - \left(\frac{\kappa_0}{\kappa}\right)^{\eta_2} e^{-\delta(\kappa - \kappa_0)},$$

where  $\eta_1$ ,  $\eta_2$  and  $\delta$  are the material constants. Equation (2.33) allows for distinguishing different stiffness degradation under tension and under compression. Damage under compression starts to develop later than under tension that is consistent with experiments. The stress-strain function is represented again by Eq. (2.3) with the term ‘ $1 - D$ ’ defined as in Abaqus [1] following LUBLINER *et al.* [32] and LEE and FENVES [29]:

$$(2.35) \quad (1 - D) = (1 - s_c D_t)(1 - s_t D_c),$$

with two splitting functions  $s_t$  and  $s_c$  controlling the magnitude of damage:

$$(2.36) \quad s_t = 1 - a_t w(\boldsymbol{\sigma}^{\text{eff}}) \quad \text{and} \quad s_c = 1 - a_c (1 - w(\boldsymbol{\sigma}^{\text{eff}})),$$

where  $a_t$  and  $a_c$  are the scale factors and  $w(\boldsymbol{\sigma}^{\text{eff}})$  denotes a stress weight function, which may be determined with the aid of principal effective stresses [29],

$$(2.37) \quad w(\boldsymbol{\sigma}^{\text{eff}}) = \begin{cases} 0 & \text{if } \boldsymbol{\sigma} = 0, \\ \frac{\sum \langle \sigma_i^{\text{eff}} \rangle}{\sum |\sigma_i^{\text{eff}}|} & \text{otherwise.} \end{cases}$$

For relatively simple cyclic tests (e.g., uniaxial tension or bending), the scale factors  $a_t$  and  $a_c$  can be equal to  $a_t = 0$  and  $a_c = 1$ , respectively. Thus, the splitting functions are:  $s_t = 1.0$  and  $s_c = w(\boldsymbol{\sigma}^{\text{eff}})$ . For uniaxial loading cases, the stress weight function becomes

$$(2.38) \quad w(\sigma^{\text{eff}}) = \begin{cases} 1 & \text{if } \sigma^{\text{eff}} > 0, \\ 0 & \text{if } \sigma^{\text{eff}} \leq 0. \end{cases}$$

Thus, under pure tension the stress weight function  $w = 1.0$  and under pure compression  $w = 0$ .

Our constitutive model with a different stiffness in tension and compression and a positive-negative stress projection operator to simulate crack closing and crack re-opening is thermodynamically consistent. It shares main properties of the model by LEE and FENVES [29], which was proved to not violate thermodynamic principles (plasticity is defined in the effective stress space, isotropic damage is used and the stress weight function is similar). Moreover, CAROL and WILLAM [11] showed that for damage models with crack closing/reopening effects included, only isotropic formulations did not suffer from spurious energy dissipation under non-proportional loading (in contrast to anisotropic ones).

Our local coupled elasto-plastic-damage model requires the following 10 material constants  $E$ ,  $\nu$ ,  $\kappa_0$ ,  $\alpha$ ,  $\beta$ ,  $\eta_1$ ,  $\eta_2$ ,  $\delta$ ,  $a_t$ ,  $a_c$  and two hardening yield stress functions (the function by Rankine in tension and by Drucker–Prager in compression). If the tensile failure prevails, one yield stress function by Rankine can be used only. The quantities  $\sigma_y$  (in the hardening function) and  $\kappa_0$  are responsible for the peak location on the stress-strain curve and a simultaneous activation of a plastic and damage criterion (usually the initial yield stress in the hardening function  $\sigma_y^0 = 3.5\text{--}6.0$  MPa and  $\kappa_0 = (8\text{--}15) \times 10^{-5}$  under tension). The shape of the stress-strain curve in softening is influenced by the constant  $\beta$  in tension (usually  $\beta = 50\text{--}800$ ), and by the constants  $\delta$  and  $\eta_2$  in compression (usually  $\delta = 50\text{--}800$  and  $\eta_2 = 0.1\text{--}0.8$ ). The parameter  $\eta_2$  influences also a hardening curve in compression. In turn, the stress-strain curve at the residual state is affected by the constant  $\alpha$  (usually  $\alpha = 0.70\text{--}0.95$ ) in tension and by  $\eta_1$  in compression (usually  $\eta_1 = 1.0\text{--}1.2$ ). Since the parameters  $\alpha$  and  $\eta_1$  are solely influenced by high values of  $\kappa$ , they can arbitrarily be assumed for softening materials. Thus, the most crucial material constants are  $\sigma_y^0$ ,  $\kappa_0$ ,  $\beta$ ,  $\delta$  and  $\eta_2$  (see Fig. 9). In turn, the scale factors  $a_t$  and  $a_c$  influence the damage magnitude in tension and compression. In general, they vary between zero and one. There do not exist, unfortunately, the experimental data allowing for determining the magnitude of  $a_t$  and  $a_c$ . Since the compressive stiffness is recovered upon the crack closure as the load changes from tension to compression and the tensile stiffness is not recovered due to compressive micro-cracks, the parameters  $a_c$  and  $a_t$  can be taken for the sake of simplicity as  $a_c = 1.0$  and  $a_t = 0$  for many different simple loading cases

as, e.g., uniaxial tension and bending. The equivalent strain measure  $\tilde{\epsilon}$  can be defined in terms of total strains or elastic strains. The drawback of our formulation (similarly as in the model ‘1’) is the necessity to tune up constants controlling plasticity and damage to activate an elasto-plastic criterion and a damage criterion at the same moment. As a consequence, the chosen yield stress  $\sigma_y$  may be higher than this obtained directly in laboratory simple monotonic experiments.

The material constants  $E, \nu, \kappa_0, \beta, \alpha, \eta_1, \eta_2, \delta$  and two hardening yield stress functions can be determined for concrete with the aid of two independent simple monotonic tests: uniaxial compression test and uniaxial tension (or three-point bending) test. However, the determination of the damage scale factors  $a_t$  and  $a_c$  requires one full cyclic compressive test and one full cyclic tensile (or three-point bending) test.

Table 1 shows a short comparison between four coupled models. The major drawback of the first three formulations is the lack of damage differentiation in tension and compression, stiffness recovery associated with crack closing and relationship between the tensile and compression stiffness during a load direction change. To describe these phenomena, additional material constants have to be included.

**Table 1. Comparison between four local coupled elasto-plastic-damage formulations to describe concrete behaviour.**

	Plastic strains in tension/compression	Stiffness degradation	Unique strain division	Stiffness recovery	Number of material parameters
Model ‘1’	Yes	Yes	No	No	Elastic: 2 Plastic: 2 (tens.) Damage: 4
Model ‘2’	Yes (only in compression)	Yes (only in tension)	Yes	No	Elastic: 2 Plastic: 3 Damage: 3-4
Model ‘3’	Yes	Yes	Yes	No	Elastic: 2 Plastic: 2 Damage: 1
Model ‘4’	Yes	Yes	No	Yes	Elastic: 2 Plastic: 1 (tension), 3 (compression) Damage: 2 (tension), 3 (compression) Scale factors: 2

The damage hardening/softening laws assumed in constitutive models have been fully based on experimental data from uniaxial compression and uniaxial tension which, in turn, strongly depend on the concrete nature, specimen size

and boundary and loading conditions. It means that they are not physically-based. This fact reveals the necessity to derive macroscopic laws in a softening regime from real micro-structure evolutions in materials during homogeneous tests using, e.g., a discrete element model [59].

The coupled model ‘1’ can be enriched by the crack-closure effect in a similar way as our model ‘4’. For the models ‘2’ and ‘3’, due to their different structure, the crack-closure effect can be incorporated by introducing a projection operator (model ‘2’) or by modifying the evolution law for the compliance tensor (model ‘3’).

### 3. Non-local theory

To describe properly strain localization, to preserve the well-posedness of the boundary value problem, to obtain FE-results free from spurious discretization sensitivity and to capture a deterministic size effect (dependence of the nominal strength on the structure size), an integral-type non-local theory is used as a regularization technique [45, 10, 3] which takes advantage of a weighted spatial averaging of a suitable state variable over a neighbourhood of each material point. Thus, stress at a certain material point depends not only on the state variable at that point but on the distribution of the state variable in a finite neighbourhood of the point considered (the principle of a local action does not hold – a non-local interaction takes place between any two points). It has a physical motivation due to the fact the distribution of stresses in the interior of concrete is strongly non-uniform due to the presence of different phases (aggregate, cement, bond). POLIZZOTTO *et al.* [47] laid down a thermodynamic consistent formulation of non-local plasticity. In turn, BORINO *et al.* [8] and NGUYEN [40] laid down a thermodynamic consistent formulation of non-local damage.

Usually, in elasto-plastic formulations, it is sufficient to achieve mesh-independent FE results to treat non-locally one state variable controlling material softening (e.g., non-local softening parameter), whereas stresses, strains and other variables remain local [10, 6]. Similarly, in isotropic scalar damage models, it is sufficient to treat a variable describing material degradation as a non-local one [36]. However in other damage formulations, this variable has to be carefully chosen because a wrong choice can cause problems with energy dissipation leading to mesh-dependent FE solutions [22, 23, 8]. This case occurred, e.g., in the coupled model ‘2’.

In the first coupled elasto-plastic-damage model (model ‘1’), the equivalent strain measure in Eq. (2.6) (describing material damage) is replaced by its non-local counterpart:

$$(3.1) \quad \bar{\varepsilon}(x_k^a) = \int_V \omega(r) \tilde{\varepsilon}(x_k) dV,$$

where  $x_k^a$  – the coordinates of the considered point (actual),  $x_k$  – the coordinates of surrounding points,  $r$  – the distance between material points,  $\omega$  – the weighting function and  $V$  – the body volume.

In the second coupled model, non-locality in tension is assigned to the energy release parameter  $Y$  (component of the loading function, Eqs. (2.16) and (2.17) to achieve a proper mesh-independent solution [35]:

$$(3.2) \quad Y = \frac{1}{2} \varepsilon_{ij} C_{ijkl}^e \varepsilon_{kl} = \sum_i^3 (-\hat{y}_{(i)}) / e^{-L}.$$

The non-local damage energy is composed of a local and non-local term calculated in the current ( $i$ ) and previous iteration ( $i - 1$ ) [49] according to [10] (see Eq. (3.5)):

$$(3.3) \quad \bar{Y}_{(i)}^* = (1 - m + mA_{kl})Y_{(i)} + m(\bar{Y}_{(i-1)} - Y_{(i-1)}A_{kl}),$$

wherein  $m$  – the non-locality parameter controlling the size of the localized plastic zone and distribution of the plastic strain and  $A_{kl}$  denotes the component of a non-local matrix (Eq. (3.8)):

$$(3.4) \quad A_{kl} = \frac{\omega(\|x^k - x^l\|)V(x^l)}{\sum_{j=1} \omega(\|x^k - x^j\|)V(x^j)}.$$

$V(x^l)$  is the volume associated with the integration point  $l$ . For the non-locality parameter  $m = 0$ , a local approach is obtained, and for  $m = 1$ , a classical non-local model is recovered. If the non-local parameter  $m > 1$ , the influence of non-locality increases and the localized plastic region reaches a finite mesh-independent size [6]. To calculate the non-local energy release parameter in Eq. (3.3), its local values were taken from the previous iteration for the sake of simplicity. Such an approximation (the values were not taken from the current iteration) does not affect the results but simultaneously reduces the calculation time [6].

In the third model, the rates of the softening parameter (Eq. (2.29)) are averaged according to [10]:

$$(3.5) \quad d\bar{\kappa}_i(x) = d\kappa_i(x) + m \left( \int \omega(x, \xi) d\kappa_i(\xi) d\xi - d\kappa_i(x) \right).$$

Since the rate of the softening parameter is not known at the iteration beginning, some extra sub-iterations are required to solve Eq. (3.5) [56]. To simplify the calculations, the non-local rates are replaced by their approximations  $d\kappa_i^{est}$  calculated on the basis of the known total strain rate [10]:

$$(3.6) \quad d\bar{\kappa}_i(x) \approx d\kappa_i(x) + m \left( \int \omega(x, \xi) d\kappa_i^{est}(\xi) d\xi - d\kappa_i^{est}(x) \right).$$

The FE-results show an insignificant influence of the calculation method of plastic rates of the non-local softening parameter [6]. In addition, an approximate method proposed by Brinkgreve in Eq. (3.6) is less time consuming (by approx. 30%). The non-local rates can be calculated in all integration points of the specimen, in the integration points where only the plastic strain occurs or only in the integration points where both plastic strain and softening occur simultaneously. However, in all these cases, the differences in results are also insignificant [6].

Finally, in the improved coupled formulation (model ‘4’), the non-locality is introduced similarly as in the model ‘1’, i.e. local plasticity is combined with non-local damage.

As a weighting function  $\omega_0$  (called also an attenuation function or a non-local averaging function), the Gauss distribution [3] is always assumed in our calculations:

$$(3.7) \quad \omega(r) = \frac{1}{c_g} e^{-(r/l_c)^2},$$

where the parameter  $l_c$  is a characteristic length of micro-structure,  $r$  is a distance between two material points and  $c_g$  denotes a normalizing factor equal to  $\sqrt{\pi}l_c$  (1D case),  $\pi l_c^2$  (2D case) and  $\pi\sqrt{\pi}l_c^3$  (3D case). The averaging in Eq. (3.7) is restricted to a small representative area around each material point (the influence of points at the distance of  $r = 3 \times l_c$  is only of 0.01%) (Fig. 1). Our non-local formulation in an integral form with the Gauss weight function does not violate thermodynamic principles [8, 23]. A characteristic length is related to the micro-structure of concrete (aggregate size). It is usually determined with an inverse identification process of experimental data [16, 33, 28, 53]. However, the determination of a representative characteristic length of micro-structure  $l_c$  is very complex in concrete since the strain localization can include a mixed mode (ten-

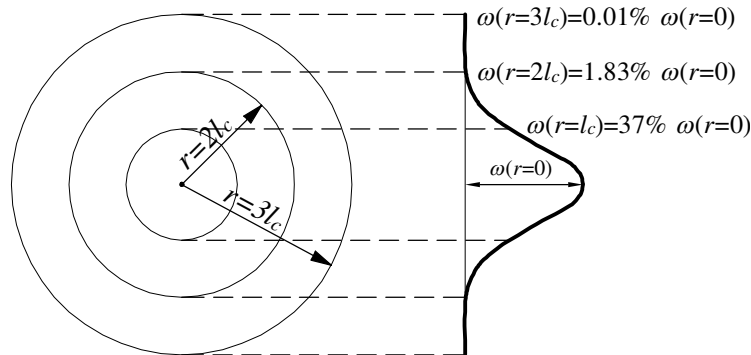


FIG. 1. Region of the influence of characteristic length  $l_c$  and weighting function  $\omega$ .

sile zones and shear zones) and a characteristic length (which is a scalar value) is related to the fracture process zone with a certain volume which changes during a deformation (the width of the fracture process zone increases according to, e.g., [46], but decreases after, e.g., [55]). In turn, other researchers conclude that the characteristic length is not a constant, and it depends on the type of the boundary value problem and the current level of damage [14]. Thus, a determination of  $l_c$  requires further numerical analysis and measurements, e.g., using a DIC technique [5, 27, 53]. Based on our both numerical simulations of concrete and reinforced concrete beams under bending and experiments using a digital image correlation DIC technique in order to measure the width of a localized zone [53, 54, 58], a characteristic length  $l_c$  of micro-structure is about 2 mm (fine-grained concrete) and 5 mm (usual concrete) within isotropic damage mechanics (using the Gauss distribution function). The setting of a direct relationship between a characteristic length  $l_c$  and concrete micro-structure (e.g., aggregate size) merits further experimental investigations [54].

A proper non-local transformation requires that a non-local field corresponding to a constant local field remains constant in the vicinity of a boundary. The applied weighting function satisfies the normalizing condition [3],

$$(3.8) \quad \omega(x, \xi) = \frac{\omega(\|x - \xi\|)}{\int_V \omega(\|x - \zeta\|) d\zeta}.$$

The algorithms for four coupled models with non-local softening are presented in Appendix. The models are implemented into the Abaqus Standard [1] program with the aid of the subroutine UMAT (user constitutive law definition) and UEL (user element definition). For the solution of a non-linear equation of motion governing the response of a system of finite elements, a modified Newton–Raphson scheme is used. The calculations are performed with a symmetric elastic global stiffness matrix instead of applying a tangent stiffness matrix (the choice was governed by access limitations to the commercial software Abaqus). The procedure yielded sufficiently accurate and fast convergence. The magnitude of the maximum out-of-balance force at the end of each calculation step was smaller than 1% of the calculated total force on the specimen. To satisfy the consistency condition  $f = 0$  in elasto-plasticity, the trial stress method (linearized expansion of the yield condition about the trial stress point) using an elastic predictor and a plastic corrector with the return mapping algorithm [41] is applied. The calculations are carried out using a large-displacement analysis. In this case, the actual configuration of the body is taken into account. The Cauchy stress is taken as the stress measure. The conjugate strain rate is the rate of deformation. The rotation of the stress and strain tensor is calculated with the Hughes–Winget method [20]. A non-local averaging is performed in the current configuration. This choice is governed by the fact that element areas

in this configuration are automatically calculated by Abaqus. The three-node triangular (with one integration point) and four-node quadrilateral (with four integration points using a selectively-reduced integration scheme) finite elements are used.

#### 4. Cyclic behaviour of concrete under tension

Due to the lack of accompanying monotonic and cyclic uniaxial laboratory tests, a general calibration procedure could not be applied to all coupled models. Therefore, the material constants in each model were found by means of preliminary FE analyses in order to satisfactorily match numerical results with experimental ones.

##### 4.1. Four-point cyclic bending of notched concrete beams

The comparative numerical plane strain simulations were performed with a concrete notched beam under four-point cycling bending subjected to tensile failure [19] (Fig. 2). The length of the beam was 0.5 m and the height 0.1 m. The deformation was induced by imposing a vertical displacement at two nodes at the top of the beam. In the calculations, the modulus of elasticity was  $E = 40$  GPa, Poisson ratio  $\nu = 0.2$  and characteristic length  $l_c = 5$  mm. The tensile strength from experiments varied between  $f_t = 2.49$  MPa and  $f_t = 4.49$  MPa. The calculations were performed with 7634 triangular finite elements. The size of elements was not greater than  $(2 - 3) \times l_c$  to obtain objective FE results [6, 36, 57]. The force-displacement diagrams  $P = f(u)$  are shown in Fig. 3. In turn, Fig. 4 presents the calculated contours of a localized zone above the notch. The evolution of non-local parameters: equivalent strain measure (models ‘1’ and ‘4’), pseudo-log damage variable (model ‘2’) and softening parameter (model ‘3’) is demonstrated in Fig. 5.

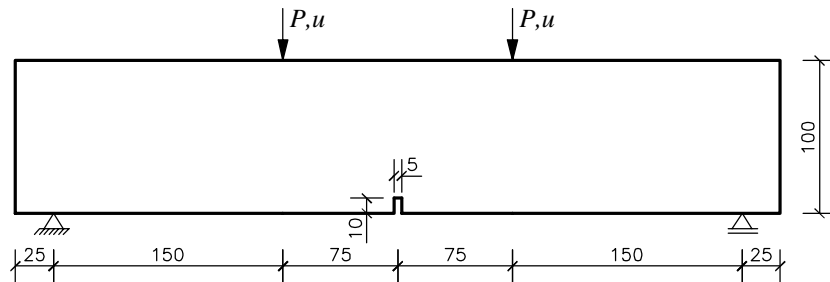


FIG. 2. Geometry of notched beam under quasi-static cyclic four-point bending ( $P$  – vertical force,  $u$  – vertical displacement) [19].

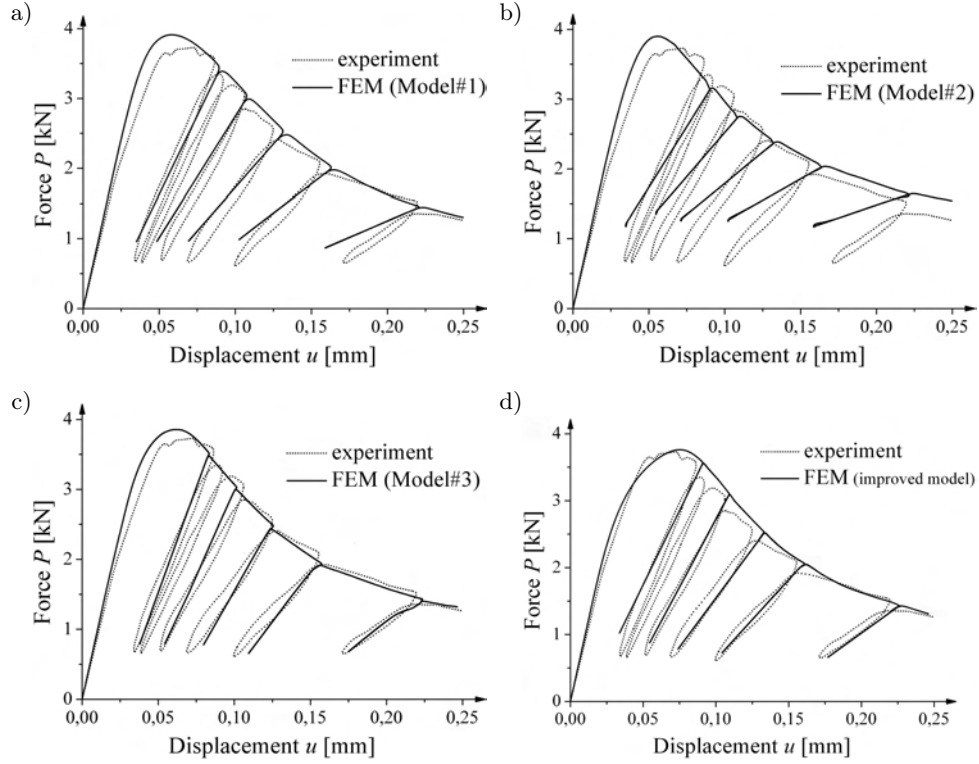


FIG. 3. Experimental and calculated force-displacement curves using four different coupled elasto-plastic-damage models with non-local softening during quasi-static four-point cyclic bending under tensile failure [19]: a) model ‘1’ (damage based on total strains), b) model ‘2’, c) model ‘3’ and d) model ‘4’ (damage based on elastic strains).

For the first enhanced coupled model (model ‘1’) with one surface in hardening plasticity, the von Mises criterion with the yield stress  $\sigma_{yt}^0 = 6.5$  MPa (total strains) and  $\sigma_{yt}^0 = 5.9$  MPa (elastic strains) was assumed with a linear hardening parameter ( $H_p = E/2$ ). Since, an elasto-plastic model is not directly responsible for the evolution of the failure mechanism, the von Mises criterion was chosen for concrete in elasto-plasticity for the sake of simplicity (the application of the criterion by Drucker–Prager does not affect FE results). The following material constants were used:  $\kappa_0 = 9.5 \times 10^{-5}$ ,  $\alpha = 0.92$  and  $\beta = 140$  with the total strains  $\tilde{\varepsilon}(\varepsilon_{ij})$ , and  $\kappa_0 = 8.6 \times 10^{-5}$ ,  $\alpha = 0.92$  and  $\beta = 170$  with the elastic strains  $\tilde{\varepsilon}(\varepsilon_{ij}^e)$ . The parameter set is different in both cases due to a varying coupling between plasticity and damage (via elastic or total strains).

Figure 3a shows the calculated load-displacement curves with a coupled elasto-plastic-damage model using total strains. The load reversals exhibit a gradual decrease of the elastic stiffness, however calculated stiffness degradation is overestimate, especially for high values of  $\kappa$ . The calculated vertical

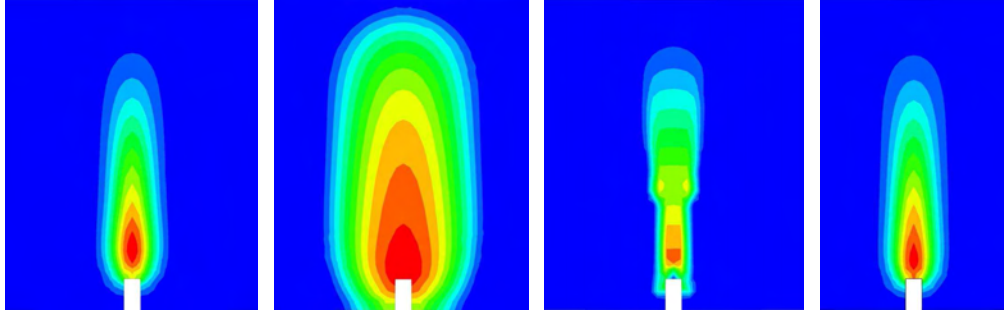


FIG. 4. Calculated contours of localized zone near notch in beam under four-point bending with four different coupled elasto-plastic-damage models with non-local softening: a) model '1', b) model '2', c) model '3' and d) model '4' (at deflection  $u = 0.15$  mm).

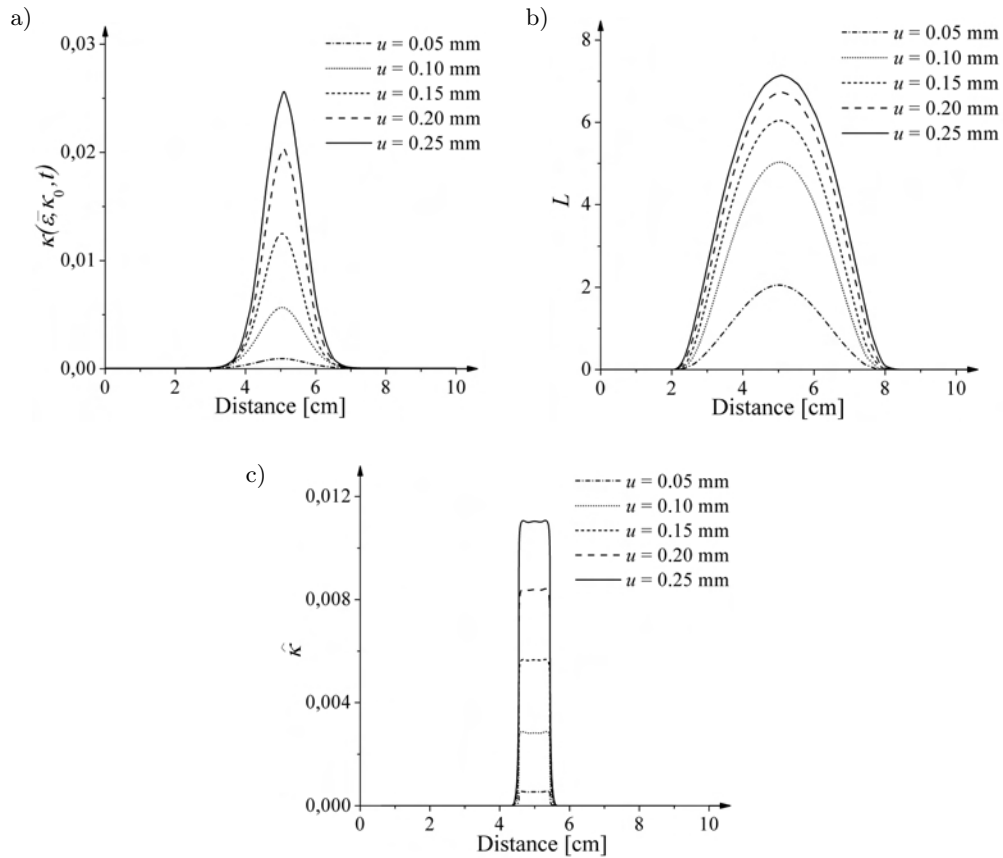


FIG. 5. Evolution of non-local parameter above notch in beam under four-point bending with 4 different coupled elasto-plastic-damage models with non-local softening: a) model '1', b) model '2' and c) model '3' (at deflection  $u = 0.15$  mm).

force is close to experiment. The slope of the load-displacement curve is realistically reflected. The width of a localized zone above the notch in the beam is about 2.4 cm ( $4.8 \times l_c$ ) (Fig. 5a).

Using the second enhanced coupled model, the resistance function by NGUYEN [39] was assumed with  $E_{pt} = 37$  GPa,  $n_t = 0.175$ ,  $f_t = 2.85$  MPa and  $m = 1.2$ . The numerical results agree well with the experimental data only in the case of the ultimate vertical force and softening slope in the post-peak regime (Fig. 3b). The calculated stiffness degradation is significantly too high than in the experiment. As a consequence, the width of a localized zone increases up to 3.2 cm ( $6.4 \times l_c$ ) (Fig. 5b). The similar results are obtained with the resistance function by Eq. (2.22).

In the third enhanced coupled model, the calculated ultimate vertical force (with the parameters:  $f_t = 2.85$  MPa,  $\kappa_0 = 1.85 \times 10^{-3}$ ,  $\gamma = 0.2$  and  $m = 2$ ) again very similar as compared with the experimental value (Fig. 3c). Also the softening behaviour is realistically reflected. The slope of the experimental and numerical curve is almost the same. The calculated stiffness degradation exhibits a proper gradual decrease and it is close to experiment. The width of the localized zone above the notch is 1.4 cm ( $2.8 \times l_c$ ) (Fig. 5c).

In the fourth enhanced model, the constants  $\sigma_{yt}^0 = 6.5$  MPa,  $H_p = E/2$ ,  $\kappa_0 = 4.3 \times 10^{-5}$ ,  $\beta = 650$ ,  $\alpha = 0.90$ ,  $\eta_1 = 1.2$ ,  $\eta_2 = 0.15$ ,  $\delta = 450$ ,  $a_t = 0$  and  $a_c = 1$  were used (damage was based on elastic strains). The calculated force-displacement curve exhibits good agreement with experimental outcomes (Fig. 3d). The bearing capacity of the beam is very well captured. The post-peak behaviour is close to experiment, however the softening slope is slightly worse reflected as in the model ‘3’. In turn, a calculated stiffness decrease is almost the same as in the experiment. Thus, an evident improvement as compared to the model ‘1’ with respect to the magnitude of the stiffness reduction was achieved. The calculated contours of a non-local variable describing the shape of a localized zone are similar as in the model ‘1’ (Fig. 4d). The results of Fig. 4 demonstrate that the shape of a localized zone above the notch is different due to the material stiffness in a softening regime induced by the material formulation. The shape of a localized zone in the models ‘1’ and ‘4’ is the same due to a similar model formulation, and is typical for other solutions within damage mechanics (e.g., [44, 42]).

Summarizing, the coupled models ‘1’, ‘3’ and ‘4’ are capable to satisfactorily capture the cyclic concrete behaviour under tensile failure.

#### 4.2. Three-point cyclic bending of notched concrete beams

In order to check the capability of the improved coupled model ‘4’ to simulate a deterministic size effect observed experimentally in brittle materials [60], the

FE-calculations were performed in addition with concrete notched beams under three-point cyclic loading (Fig. 6, Table 2) [43]. The number of triangular finite elements was equal to 2.292, 5.213 and 9.211 for a small-, medium- and large-size beam, respectively. The size of elements was again not greater than  $3 \times l_c$ . The deformation was induced by imposing a vertical displacement at the mid-node at the beam top. The modulus of elasticity was  $E = 45.6$  GPa and the Poisson ratio was  $\nu = 0.2$  and. To match approximately the numerical results with the experimental ones, the following material constants were chosen for three beams:  $\sigma_{yt}^0 = 6.5$  MPa,  $H_p = E/2$ ,  $\kappa_0 = 9.0 \times 10^{-5}$ ,  $\beta = 1550$ ,  $\alpha = 0.99$ ,  $\eta_1 = 1.2$ ,  $\eta_2 = 0.15$ ,  $\delta = 950$ ,  $a_t = 0$  and  $a_c = 1$  and  $l_c = 5$  mm (equivalent strain measure based on elastic strains). As compared to FE calculations at four-point cyclic bending, the same constants  $\sigma_y$ ,  $H_p$ ,  $\eta_1$ ,  $\eta_2$ ,  $a_t$  and  $a_c$  were assumed.

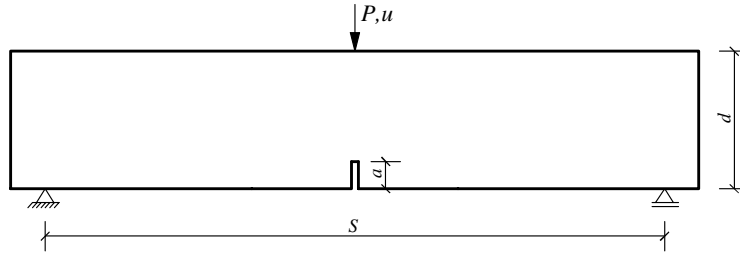


FIG. 6. Geometry of notched beam under quasi-static cyclic three-point bending ( $P$  – vertical force,  $u$  – deflection, dimensions are given in Table 2) [43].

**Table 2. Concrete beam dimensions in quasi-static cyclic tests by PERDIKARIS and ROMEO [43] (Fig. 6).**

Beam	Height $d$ [mm]	Thickness $t$ [mm]	Span $S$ [mm]	Notch height $a$ [mm]
small	64	127	254	20
medium	128	127	508	39
large	254	127	1016	78

Figures 7a and 7b demonstrate the calculated force-displacement diagrams for a small- and large-size beam compared with the experimental data. The stiffness degradation is again realistically captured by the model. The calculated ultimate force as compared to experiments is higher by 10–15%. To obtain a better agreement between ultimate forces and calculated stiffness, the material constant should be better calibrated (in particular  $\kappa_0$  and parameters controlling the damage evolution  $\beta$ ,  $\delta$  and  $\eta_2$ ). The calculated results of a deterministic size

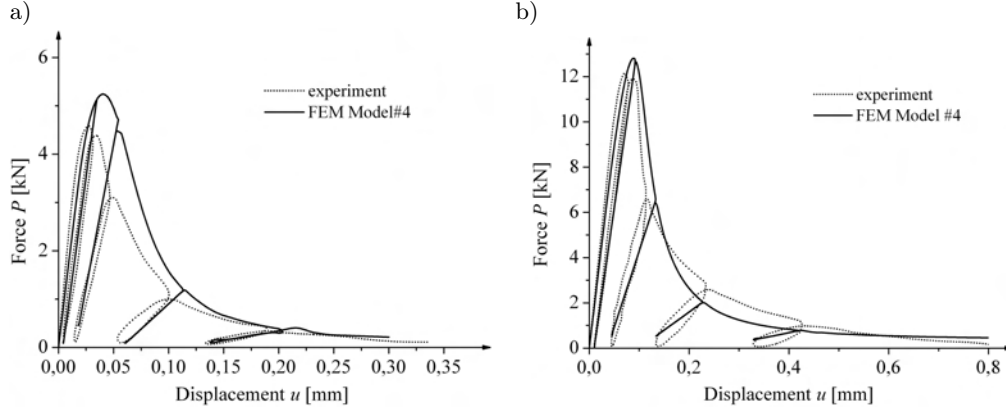


FIG. 7. Experimental [43] and calculated load-displacement curves with enhanced coupled model '4' with damage based on elastic strains (quasi-static cyclic three-point bending): a) small-size beam, b) large-size beam ( $a_t = 0.0$  and  $a_c = 1.0$ ).

effect with respect to the ultimate vertical force were confronted with the size effect law by BAŽANT [2, 4] for notched beams:

$$(4.1) \quad \sigma_N = \frac{B f_t}{\sqrt{1 + D/D_0}},$$

wherein  $\sigma_N$  – the nominal strength,  $f_t$  – the tensile strength,  $D$  – the specimen characteristic size equal to the beam height),  $B$  – the dimensionless geometry-dependent parameter (depending on the geometry of the structure and crack) and  $D_0$  – the size-dependent parameter called transitional size (both unknown parameters to be determined). The FE results of the normalized vertical force versus  $d/l_c$  (Fig. 8) indicate a satisfactory agreement with Eq. (4.1) (the results

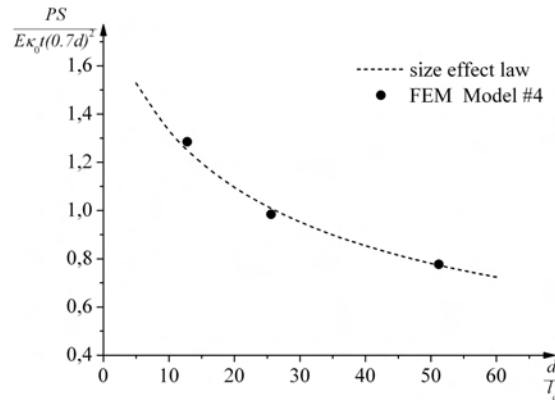


FIG. 8. Calculated deterministic size effect for concrete notched beams subjected to quasi-static cyclic three-point bending (using coupled model '4') as compared with size effect law by BAŽANT [4] ( $t$  – beam thickness,  $d$  – beam height,  $S$  – beam span).

of FE calculations on size effect with larger concrete notched beams are given by BOBIŃSKI *et al.* [7]).

## 5. Cyclic behaviour of concrete under compression and tension

First, simple cyclic uniaxial element tests were numerically performed to show the behaviour of the model ‘4’ (with four-node quadrilateral elements). Figure 9 shows the load-displacement diagrams under cyclic uniaxial tension and cyclic uniaxial compression for different influential material constants  $\beta$ ,  $\delta$ ,  $\eta_2$  and  $\kappa_0$  (which were independently changed). The effect of the constant  $\alpha$  ( $\alpha = 0.7\text{--}0.99$ ) and  $\eta_1$  ( $\eta_1 = 1.0\text{--}1.2$ ) was negligible (Sec. 2.4). The modulus of elasticity was  $E = 40$  GPa and the Poisson ratio was  $\nu = 0.18$ . In tension,  $\sigma_{yt}^0 = 4.0$  MPa and  $H_p = E/2$  (Rankine criterion), and in compression  $\sigma_{yc}^0 = 40$  MPa,  $H_p = E/2$ ,  $\phi = 20^\circ$  and  $\psi = 10^\circ$  (Drucker–Prager criterion) were chosen. The equivalent strain measure was based on total strains. The material constants varied in the following ranges:  $\beta = 200\text{--}1100$ ,  $\delta = 200\text{--}900$ ,

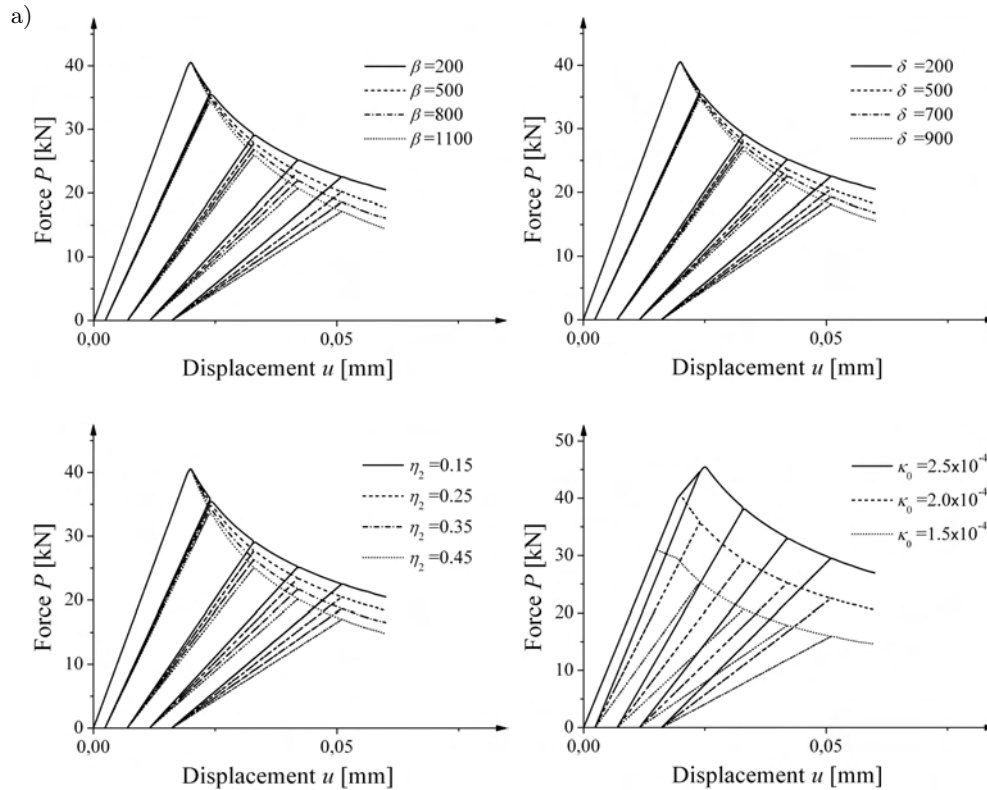


FIG. 9. Effect of different material constants on uniaxial response of coupled elasto-plastic-damage model ‘4’ for concrete under: a) cyclic uniaxial tension.

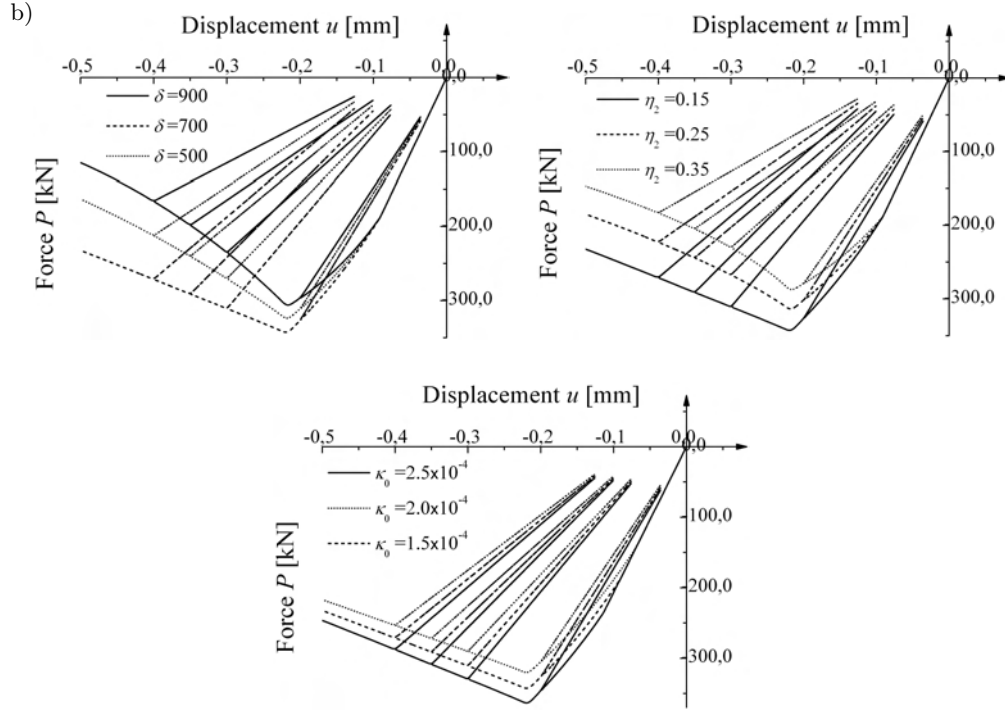


FIG. 9. (c.d) Effect of different material constants on uniaxial response of coupled elasto-plastic-damage model '4' for concrete under: b) cyclic uniaxial compression (with damage scale factors  $a_t = 0.0$  and  $a_c = 1.0$ ).

$\eta_2 = 0.15-0.45$  and  $\kappa_0 = (15-25) \times 10^{-5}$  (with  $\alpha = 0.95$ ,  $\eta_1 = 1.2$ ,  $a_t = 0.0$  and  $a_c = 1.0$ ). The force-displacement results indicate that the effect of  $\kappa_0$ ,  $\beta$ ,  $\delta$  and  $\eta_2$  is significant in tension and the effect of  $\kappa_0$ ,  $\delta$  and  $\eta_2$  is pronounced in compression. The parameter  $\kappa_0$  is responsible for a peak location and a simultaneous activation of a plastic and damage criterion. The parameters  $\beta$ ,  $\delta$  and  $\eta_2$  affect a model response in softening during tension and compression, and the parameter  $\eta_2$  influences a hardening curve in compression. The effect of two other parameters ( $\alpha$  and  $\eta_1$ ) describing the stress-strain curve at the residual state is negligible.

Next, a simple cyclic tension-compression-tension element test was calculated (Fig. 10) ( $\sigma_{yt}^0 = 4$  MPa,  $\sigma_{yc}^0 = 40$  MPa,  $H_p = E/2$ ,  $\phi = 20^\circ$ ,  $\psi = 10^\circ$ ,  $\beta = 550$ ,  $\delta = 950$ ,  $\kappa_0 = 8.5 \times 10^{-5}$ ,  $\alpha = 0.95$ ,  $\eta_1 = 1.2$ ,  $\eta_2 = 0.15$ ,  $a_t = 0.0$  and  $a_c = 1.0$ ). The results show obviously the different stiffness degradation during compression and tension (that is stronger in tension). A recovery of the compressive stiffness upon crack closure and un-recovery of the tensile stiffness as the load changes between tension and compression is satisfactorily reflected. The evident difference between a pure damage model (without plastic strains) and

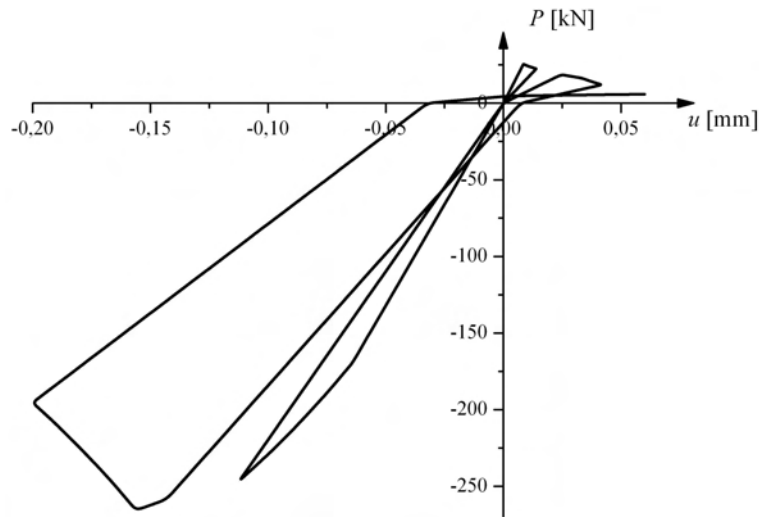


FIG. 10. Calculated load-displacement curve with coupled model '4' (with damage scale factors  $a_t = 0.0$  and  $a_c = 1.0$ ) during uniaxial tension-compression-tension.

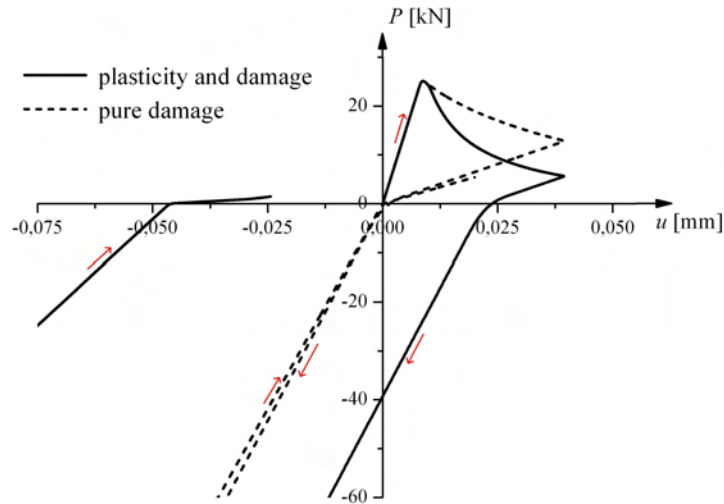


FIG. 11. Calculated load-displacement curves with coupled model '4' during uniaxial tension-compression-tension with and without plastic strains (in the load range from  $-60$  up to  $20$  kN).

coupled one (with plastic strains) during one uniaxial load cycle is demonstrated in Fig. 11.

The effect of the damage scale factors  $a_t$  and  $a_c$  on the load-displacement diagram under tension-compression-tension is described in Fig. 12 by assuming  $a_t = 0.2$  and  $a_c = 0.8$ . This change of both factors is stronger in compression.

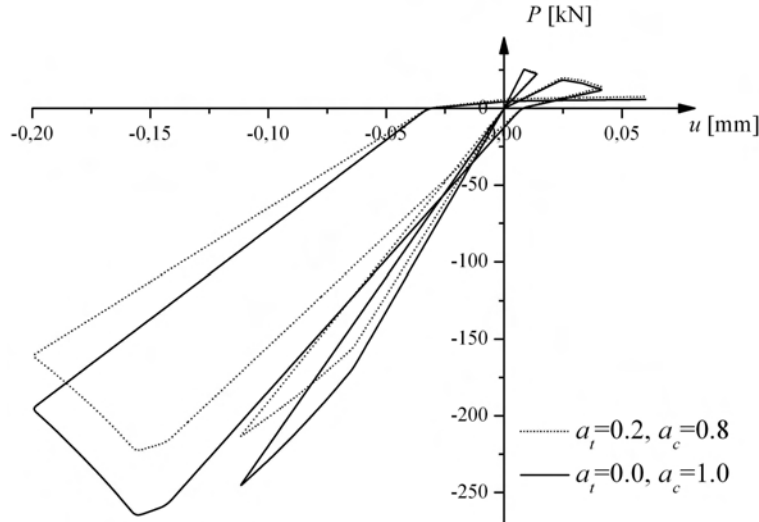


FIG. 12. Uniaxial response of coupled elasto-plastic-damage model '4' for concrete under tension-compression-tension for different damage scale factors  $a_t$  and  $a_c$ .

Finally, Fig. 13 demonstrates the 2D FE results with the model '4' for a concrete specimen subjected to uniaxial cyclic compression by taking strain localization into account. All nodes at the lower edge of a rectangular specimen were fixed in a vertical direction. The size of the specimen was arbitrarily chosen: 15 cm (height) and 5 cm (width). To preserve the stability of the specimen, the node in the middle of the lower edge was kept fixed. The deformations were initiated through constant vertical displacement increments prescribed to nodes along the upper edge of the specimen. The lower and upper edges were smooth. The number of triangular finite elements was 896 (the size of elements was not greater than  $3 \times l_c$ ). The material constants were:  $E = 30$  GPa,  $\nu = 0.18$ ,  $\sigma_{yc}^0 = 20$  MPa,  $\phi = 25^\circ$ ,  $\psi = 10^\circ$ ,  $\eta_1 = 1.2$ ,  $\eta_2 = 0.7$ ,  $\delta = 800$ ,  $l_c = 5$  mm,  $a_t = 0.0$  and  $a_c = 1.0$ . To induce strain localization, a weak element was inserted in the middle of height, on the edge of the specimen. Due to the lack of the initial experimental data, the calculated stress-strain curve was qualitatively compared with the experimental one by KARSAN and JIRSA [25] (Fig. 13).

The calculated stress-strain curve (Figs. 13c and 13d) is qualitatively the same as in a cyclic compressive test by KARSAN and JIRSA [25] (Figs. 13c and 13e) with respect to material softening and stiffness degradation. The calculated thickness of a localized zone is 3.4 cm ( $6.8 \times l_c$ ) and the inclination to the horizontal is about  $45^\circ$  (Fig.13b). These results are very similar as those within elasto-plastic calculations [6]. The shear zone inclination is significantly higher

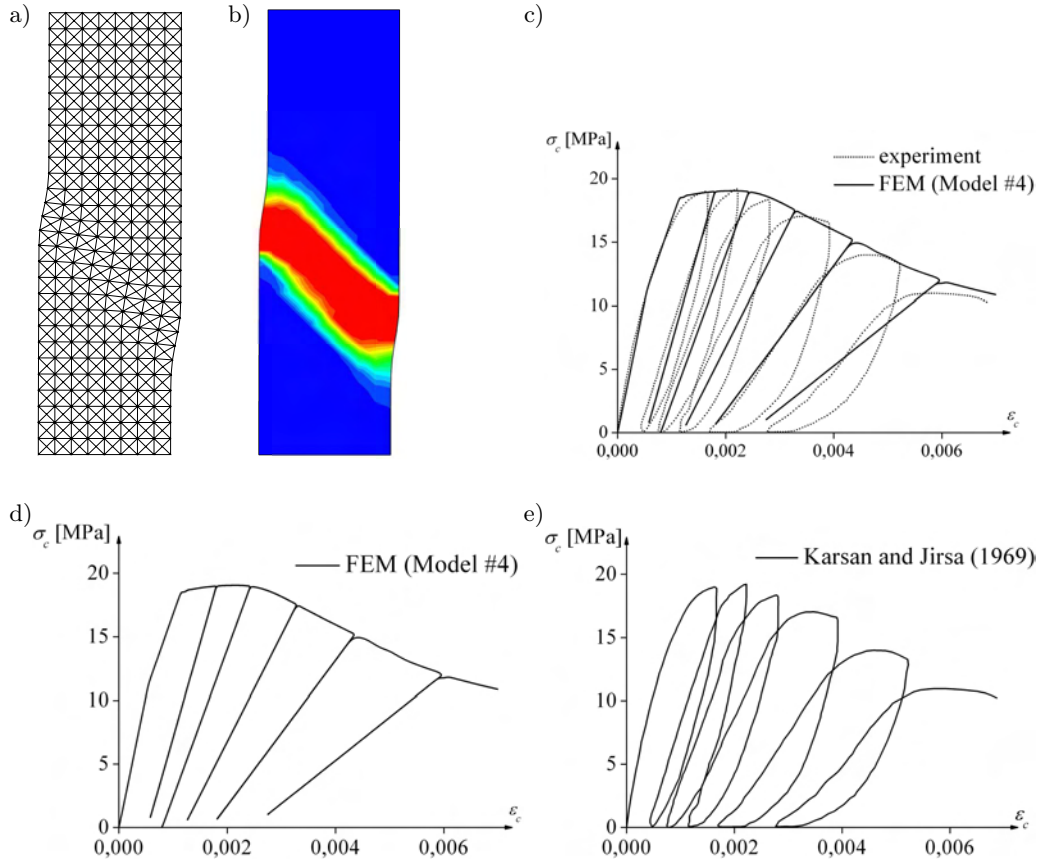


FIG. 13. Response of coupled elasto-plastic-damage model ‘4’ for concrete specimen under uniaxial cyclic compression from FE calculations (with damage scale factors  $a_t = 0.0$  and  $a_c = 1.0$ ): a) deformed FE mesh, b) contours of calculated non-local parameter, c) calculated and experimental stress-strain curve by KARSAN and JIRSA [25], d) calculated stress-strain curve, e) experimental stress-strain curve by KARSAN and JIRSA [25].

(and more realistic) than the one obtained with a simple non-local isotropic damage model [52], that was smaller than  $35^\circ$ – $40^\circ$ .

## 6. Conclusions

The presented FE calculations show that all coupled elasto-plastic-damage models enhanced by a characteristic length of micro-structure in a softening regime can properly reproduce the experimental load-displacement diagrams and strain localization in plain concrete notched beams under tensile loading during quasi-static cyclic bending. All models ‘1-4’ properly capture material softening and the width of a localized zone. The models ‘1’, ‘3’ and ‘4’ are also able

to correctly describe the stiffness degradation. The drawback of the model ‘2’ is the lack of possibility to simulate simultaneously both plastic deformation and stiffness degradation during cyclic loading. The model ‘3’ has the smallest number of material constants to be calibrated. The coupled models ‘3’ and ‘4’ indicate the best agreement with cyclic bending experiments under tensile failure. In general, the models 1, 3 and 4 show similar results under tension. The shape and thickness of a localized zone above the notch in concrete beams under tension depends on the coupled formulation.

A choice of a suitable local state variable for non-local averaging is strongly dependent upon the model. It should be carefully checked to avoid problems with non-sufficient regularization.

The improved model ‘4’ captures, in addition, plastic strains and stiffness degradation in both tension and compression, and stiffness recovery effect during cyclic loading by means of a strain equivalence hypothesis (thus the coupling between damage and plasticity is different than in Abaqus 2004). It is able to properly describe strain localization under both tension and compression due to a presence of a characteristic length of micro-structure. Its drawback is no clear distinction between elastic, plastic and damage strain rates, and a relatively large number of material constants to be calibrated. Most of material constants may be calibrated independently with a monotonic uniaxial compression and tension (bending) test. Standard uniaxial cyclic tests are needed to calibrate damage scale factors.

## Acknowledgment

Research work has been carried out within the project: “Innovative ways and effective methods of safety improvement and durability of buildings and transport infrastructure in the sustainable development” financed by the European Union. The numerical calculations were performed on supercomputers of the Academic Computer Centre in Gdańsk TASK.

## Appendix

### Algorithm for coupled model ‘1’

#### Stage 1

For each integration point

- 1) Compute strain increments  $\Delta\varepsilon_{ij}$  and update total strains  $\varepsilon_{ij}$   
(elastic predictor)  
 $(\varepsilon_{ij}^e)^{\text{trial}} = (\varepsilon_{ij}^e)^t + \Delta\varepsilon_{ij}$  and  $(\varepsilon_{ij}^p)^{\text{trial}} = (\varepsilon_{ij}^p)^t$
- 2) Compute stress (elastic predictor)  
 $\tilde{\sigma}_{ij}^{\text{trial}} = \tilde{\sigma}_{ij}^t + C_{ijkl}^e \Delta\varepsilon_{kl}$

- 3) Check  
 if  $F(\tilde{\sigma}_{ij}^{\text{trial}}, \kappa^t) \geq 0$  (plasticity)  
 initialization  $\tilde{\sigma}_{ij}^{(0)} = \tilde{\sigma}_{ij}^{\text{trial}}, \Delta\kappa^{(0)} = 0, i = 0$   
 while  $|F(\tilde{\sigma}_{ij}^{(i+1)}, \kappa^t + \Delta\kappa^{(i+1)})| \leq 10^{-10}$   
 a) compute  $\delta\lambda$  and  $\Delta\kappa^{(i+1)}$   
 b) update stress  $\tilde{\sigma}_{ij}^{(i)} \rightarrow \tilde{\sigma}_{ij}^{(i+1)}$  end while  
 else (elasticity):  $\kappa^{t+\Delta t} = \kappa^t, \tilde{\sigma}_{ij}^{t+\Delta t} = \tilde{\sigma}_{ij}^{\text{trial}}, (\varepsilon_{ij}^e)^{t+\Delta t} = (\varepsilon_{ij}^e)^{\text{trial}}, (\varepsilon_{ij}^p)^{t+\Delta t} = (\varepsilon_{ij}^p)^{\text{trial}}$

Choice if  $\tilde{\varepsilon} \rightarrow \tilde{\varepsilon}((\varepsilon_{ij}^e)^{t+\Delta t})$  or  $\tilde{\varepsilon} \rightarrow \tilde{\varepsilon}((\varepsilon_{ij}^p)^{t+\Delta t})$

### Stage 2

For each integration point

- 1) Compute non-local value of equivalent strain measure  $\tilde{\varepsilon} \rightarrow \bar{\varepsilon}^{(1)}$
- 2) Update the damage threshold parameter  $\kappa(t) \rightarrow \kappa(t + \Delta t)$   
 $\kappa = \max\{\max_{\tau \leq t} \bar{\varepsilon}(\tau), \kappa_0\}$
- 3) Check  
 if  $f(\bar{\varepsilon}, \kappa(t + \Delta t)) \geq 0$   
 update damage variable:  $D^t \rightarrow D^{t+\Delta t}$   
 else  $D^{t+\Delta t} = D^t$
- 4) Update stress  
 $\sigma_{ij}^{t+\Delta t} = (1 - D^{t+\Delta t})\tilde{\sigma}_{ij}^{t+\Delta t}$

<sup>(1)</sup>Calculation of non-local equivalent strain measure (Eq. (3.1)) in surrounding integration points.

### Algorithm for coupled model '2'

For each integration point

- 1) Compute strain increments  $\Delta\varepsilon_{ij}$  and update total strains  $\varepsilon_{ij}$   
 $(\varepsilon_{ij}^e)^{t+\Delta t} = (\varepsilon_{ij}^e)^t + \Delta\varepsilon_{ij}$
- 2) Compute effective strain (trial)  
 $(\tilde{\varepsilon}_{ij})^{t+\Delta t} = \exp(-L^t/2)(\varepsilon_{ij})^{t+\Delta t}$
- 3) Compute effective stress (trial)  
 $(\tilde{\sigma}_{ij}) = C_{ijkl}^e(\tilde{\varepsilon}_{kl})^{t+\Delta t}$
- 4) Compute non-local damage energy release  $\bar{Y}^*$  <sup>(1)</sup>
- 5) Check  
 if  $f(\bar{Y}^*) - r(L^{t+\Delta t}) \geq 0$   
 initialization:  $f^{(0)} = f(\bar{Y}^*), \Delta L^{(0)} = 0, i = 0$   
 while  $|f(\bar{Y}^*)^{(i+1)} - r(L^t + \Delta L^{(i+1)})| \leq 10^{-10}$   
 a) compute:  $\delta L$  and  $\Delta L^{(i+1)}$   
 b) update loading function:  $f(\bar{Y}^*)^{(i+1)}$   
 end while  
 else:  $L^{t+\Delta t} = L^t$
- 6) Update secant stiffness  
 $(C_{ijkl}^s)^{t+\Delta t} = \exp(-L^{t+\Delta t})C_{ijkl}^e$
- 7) Update stress  
 $\sigma_{ij}^{t+\Delta t} = (C_{ijkl}^s)^{t+\Delta t}(\varepsilon_{kl})^{t+\Delta t}$

<sup>(1)</sup>Calculation of non-local damage energy release (Eq. (3.3)) in surrounding integration points in current and previous iteration.

**Algorithm for coupled model ‘3’**

For each integration point

- 1) Compute strain increments  $\Delta\varepsilon_{ij}$  and update total strain  $\varepsilon_{ij}$   
(elastic predictor)  
 $(\varepsilon_{ij}^e)^{\text{trial}} = (\varepsilon_{ij})^t + \Delta\varepsilon_{ij} - (\varepsilon_{ij}^p)^t$
  - 2) Compute stress  
 $\sigma_{ij}^{\text{trial}} = (C_{ijkl})^t (\varepsilon_{kl}^e)^{\text{trial}}$
  - 3) Compute approximation of the softening parameter  $\Delta\kappa^{\text{est}}$  <sup>(1)</sup>
  - 4) Check  
if  $f(\sigma_{ij}^{\text{trial}}, \kappa^t + \Delta\tilde{\kappa}) \geq 0$ , where  $\Delta\tilde{\kappa} = m(\sum a_k \Delta\kappa_k^{\text{est}} - \Delta\kappa^{\text{est}})$  <sup>(2)</sup>  
while  $|f(\sigma_{ij}^{(i+1)}, \kappa^t + (\Delta\hat{\kappa})^{(i+1)})| \leq 10^{-10}$ 
    - a) initialization:  $\sigma_{ij}^{(0)} = \sigma_{ij}^{\text{trial}}$ ,  $\Delta\kappa^{(0)} = 0$ ,  $i = 0$
    - b) compute rate of non-local softening parameter:  
 $\Delta\hat{\kappa}^{(i+1)} = \Delta\kappa^{(i+1)} + m(\sum a_k \Delta\kappa_k^{\text{est}} - \Delta\kappa^{\text{est}})$  <sup>(3)</sup>
    - c) update stress:  $\sigma_{ij}^{(i)} \rightarrow \sigma_{ij}^{(i+1)}$
- end while  
update strain  
 $(\varepsilon_{ij}^p)^{t+\Delta t} = (\varepsilon_{ij}^p)^t + (\Delta\varepsilon_{ij}^p)^{t+\Delta t}$ ,  $(\varepsilon_{ij}^d)^{t+\Delta t} = (\varepsilon_{ij}^d)^t + (\Delta\varepsilon_{ij}^d)^{t+\Delta t}$  according to Eq. (2.27)  
and  $(\varepsilon_{ij}^e)^{t+\Delta t} = (\varepsilon_{ij}^e)^{\text{trial}} - (\Delta\varepsilon_{ij}^p + \Delta\varepsilon_{ij}^d)^{t+\Delta t}$   
update compliance tensor  $(D_{ijkl})^t \rightarrow (D_{ijkl})^{t+\Delta t}$  according to Eq. (2.28)  
else (elasticity):  
 $\kappa^{t+\Delta t} = \kappa^t$ ,  $\sigma_{ij}^{t+\Delta t} = \sigma_{ij}^{\text{trial}}$ ,  $(\varepsilon_{ij}^e)^{t+\Delta t} = (\varepsilon_{ij}^e)^{\text{trial}}$ ,  $(\varepsilon_{ij}^p)^{t+\Delta t} = (\varepsilon_{ij}^p)^t$ ,  $(\varepsilon_{ij}^d)^{t+\Delta t} = (\varepsilon_{ij}^d)^t$   
and  $(D_{ijkl})^{t+\Delta t} = (D_{ijkl})^t$
- <sup>(1)</sup> Approximation  $\Delta\kappa^{\text{est}}$  is calculated on the basis of known total strain rate.  
<sup>(2)</sup> Rate of non-local softening parameter is calculated by Eq. (3.6) with approximation  $\Delta\kappa^{\text{est}}$  in surrounding integration points in current iteration.  
<sup>(3)</sup>  $a_k$  is element of nonlocal coefficient matrix (Eq. (3.4)) in row associated with considered integration point.

**Algorithm for coupled model ‘4’**
**Stage 1**

For each integration point

Step 1) to 3) identically as in model ‘1’

Choice if  $\tilde{\varepsilon} \rightarrow \tilde{\varepsilon}((\varepsilon_{ij}^e)^{t+\Delta t})$  or  $\tilde{\varepsilon} \rightarrow \tilde{\varepsilon}((\varepsilon_{ij})^{t+\Delta t})$

**Stage 2**

For each integration point

- 1) Compute non-local value of equivalent strain measure  $\tilde{\varepsilon} \rightarrow \bar{\varepsilon}$  <sup>(1)</sup>
- 2) Update the damage threshold parameter  $\kappa(t) \rightarrow \kappa(t + \Delta t)$   
 $\kappa = \max\{\max_{\tau \leq t} \bar{\varepsilon}(\tau), \kappa_0\}$
- 3) Check  
if  $f(\bar{\varepsilon}, \kappa(t + \Delta t)) \geq 0$   
update damage variable:
  - calculate damage evolution in tension and compression (Eqs. (2.8) and (2.34))
  - calculate stress weight factor according to Eq. (2.38)
  - evaluate stiffness recovery functions according to Eq. (2.36)

– update component ‘1-D’:  $(1 - D)^t \rightarrow (1 - D)^{t+\Delta t}$  (Eq. (2.35))  
 else:  $(1 - D)^{t+\Delta t} = (1 - D)^t$

4) Update stress  
 $\sigma_{ij}^{t+\Delta t} = (1 - D)^{t+\Delta t} \bar{\sigma}_{ij}^{t+\Delta t}$

<sup>(1)</sup>Calculation of non-local equivalent strain measure (Eq. (3.1)) with in-surrounding integration points.

## References

1. *Abaqus, Theory Manual*, Version 5.8, Hibbit, Karlsson & Sorensen Inc., 2004.
2. Z. P. BAŽANT, J. PLANAS, *Fracture and size effect in concrete and other quasibrittle materials*, CRC Press, 1998.
3. Z. P. BAŽANT, M. JIRÁSEK, *Nonlocal integral formulations of plasticity and damage: survey of progress*, J. Engng. Mech., **128**, 11, 1119–1149, 2002.
4. Z. P. BAŽANT, *Scaling of Structural Strength*, Hermes-Penton, London, 2003.
5. A. R. BHANDARI, J. INOUE, *Experimental study of strain rates effects on strain localization characteristics of soft rocks*, Soils and Foundations, **45**, 1, 125–140, 2005.
6. J. BOBIŃSKI, J. TEJCHMAN, *Numerical simulations of localization of deformation in quasi-brittle materials within non-local softening plasticity*, Computers and Concrete, **4**, 433–455, 2004.
7. J. BOBIŃSKI, J. TEJCHMAN, J. GÓRSKI, *Notched concrete beams under bending - calculations of size effects within stochastic elasto-plasticity within non-local softening*, Archives of Mechanics, **61**, 3–4, 1–25, 2009.
8. G. BORINO, B. FAILLA, F. PARRINELLO, *A symmetric nonlocal damage theory*, Int. J. Solids Struct., **40**, 3621–3645, 2003.
9. R. DE BORST, L. J. SLUYS, H.-B. MÜHLHAUS, J. PAMIN, *Fundamental issues in finite element analysis of localization of deformation*, Engineering Computations, **10**, 99–121, 1993.
10. R. B. BRINKGREVE, *Geomaterial models and numerical analysis of softening*, PhD Thesis, Delft University of Technology, Delft, 1994.
11. I. CAROL, K. WILLAM, *Spurious energy dissipation/generation in stiffness recovery models for elastic degradation and damage*, Int. J. Solids Structures, **33**, 20–22, 2939–2957, 1996.
12. I. CAROL, E. RIZZI, K. WILLAM, *On the formulation of anisotropic elastic degradation*, Int. J. of Solids and Structures, **38**, 491–518, 2001.
13. J. CHEN, H. YUAN, D. KALKHOF, *A nonlocal damage model for elastoplastic materials based on gradient plasticity theory*, Report Nr. 01-13, Paul Scherrer Institute, 1–130, 2001.
14. I. FERRARA, M. DI PRISCO, *Mode I fracture behaviour in concrete: nonlocal damage modeling*, ASCE Journal of Engineering Mechanics, **127**, 7, 678–692, 2001.
15. M. G. D. GEERS, *Experimental analysis and computational modeling of damage and fracture*, PhD Thesis, Eindhoven University of Technology, Eindhoven, 1997.

16. M. GEERS, T. PEIJS, W. BREKELMANS, R. DE BORST, *Experimental monitoring of strain localization and failure behaviour of composite materials*, Compos. Sci. Technol., **56**, 1283–1290, 1996.
17. N. R. HANSEN, H. L. SCHREYER, *A thermodynamically consistent framework for theories of elasto-plasticity coupled with damage*, Int. J. of Solid Structures, **31**, 3, 359–389, 1994.
18. E. HANSEN, K. WILLAM, *A two-surface anisotropic damage-plasticity model for plane concrete*, proceedings Int. Conf. Fracture Mechanics of Concrete Materials, R. DE BORST [Ed.], Paris, Balkema, 549–556, 2001.
19. D. A. HORDIJK, *Local approach to fatigue of concrete*, PhD Thesis, Delft University of Technology, 1991.
20. T. J. R. HUGHES, J. WINGET, *Finite rotation effects in numerical integration of rate constitutive equations arising in large deformation analysis*, Intern. Journal for Numerical Methods in Engineering, **15**, 1862–1867, 1980.
21. A. IBRAHIMBEGOVIC, D. MARKOVIC, F. GATUING, *Constitutive model of coupled damage-plasticity and its finite element implementation*, Eur. J. Finite Elem., **12**, 4, 381–405, 2003.
22. M. JIRÁSEK, *Nonlocal models for damage and fracture: comparison of approaches*, Int. J. of Solids and Structures, **35**, 31–32, 4133–4145, 1998.
23. M. JIRÁSEK, S. ROLSHOVEN, *Comparison of integral-type nonlocal plasticity models for strain-softening materials*, Int. J. of Engineering Science, *41*, 13–14, 1553–1602, 2003.
24. L. M. KACHANOV, *Introduction to Continuum Damage Mechanics*, Dordrecht, Martinus Nijhoff, 1986.
25. D. KARSAN, J. O. JIRSA, *Behavior of concrete under compressive loadings*, J. Struct. Div. ASCE **95**, ST12, 2543–2563, 1969.
26. M. KLISIŃSKI, Z. MRÓZ, *Description of non-elastic deformation and damage of concrete*, script, Technical University of Poznań, Poznań, 1988 [in polish].
27. J. KOZICKI, J. TEJCHMAN, *Experimental investigations of strain localization in concrete using Digital Image Correlation (DIC) technique*, Archives of Hydro-Engineering and Environmental Mechanics, **54**, 1, 3–24, 2007.
28. C. LE BELLEGO, J. F. DUBE, G. PIJAUDIER-CABOT, B. GERARD, *Calibration of nonlocal damage model from size effect tests*, E. J. Mechanics A/Solids, **22**, 33–46, 2003.
29. J. LEE, G. L. FENVES, *Plastic-damage model for cyclic loading of concrete structures*, Journal of Engineering Mechanics, **124**, 8, 892–900, 1998.
30. J. LEE, G. L. FENVES, *A plastic-damage concrete model for earthquake analysis of dams*, Earthquake Engng. and Struct. Dyn., **27**, 937–956, 1998.
31. J. LEMAITRE, *Coupled elasto-plasticity and damage constitutive equations*, Computer Methods Appl. Mech. Eng., **51**, 31–49, 1985.
32. J. LUBLINER, J. OLIVER, S. OLLER, E. ONATE, *A plastic-damage model for concrete*, Int. J. of Solids Struct., **25**, 3, 229–326, 1989.
33. R. MAHNKEN, E. KUHL, *Parameter identification of gradient enhanced damage models*, Eur. J. Mech. A/Solids, **18**, 819–835, 1999.

34. T. MAJEWSKI, J. BOBIŃSKI, J. TEJCHMAN, *FE-analysis of failure behaviour of reinforced concrete columns under eccentric compression*, Engineering Structures, **30**, 2, 300–317, 2008.
35. I. MARZEC, *Application of coupled elasto-plastic-damage models with non-local softening to concrete cyclic behavior*, PhD Thesis, Gdańsk University of Technology, 2009.
36. I. MARZEC, J. BOBIŃSKI, J. TEJCHMAN, *Simulations of spacing of localized zones in reinforced concrete beams using elasto-plasticity and damage mechanics with non-local softening*, Computers and Concrete, **4**, 5, 377–402, 2007.
37. J. MAZARS, *A description of micro- and macroscale damage of concrete structures*, J. Engrg. Fracture Mech., **25**, 5/6, 729–737, 1986.
38. G. MESCHKE, R. LACKNER, H. A. MANG, *An anisotropic elastoplastic-damage model for plain concrete*, Int. J. for Numerical Methods in Engineering, **42**, 4, 702–727, 1998.
39. G. D. NGUYEN, *A thermodynamic approach to constitutive modelling of concrete using damage mechanics and plasticity theory*, PhD Thesis, Trinity College, University of Oxford, 2005.
40. G. D. NGUYEN, *A thermodynamic approach to non-local damage modelling of concrete*, International Journal of Solids and Structures, **45**, 7–8, 1918–1934, 2008.
41. M. ORTIZ, I. C. SIMO, *An analysis of a new class of integration algorithms for elasto-plastic constitutive relation*, Int. I. Num. Methods in Engrg., **23**, 353–366, 1986.
42. J. PAMIN, R. DE BORST, *Stiffness degradation in gradient-dependent coupled damage-plasticity*, Archives of Mechanics, **51**, 3–4, 419–446, 1999.
43. P. C. PERDIKARIS, A. ROMEO, *Size effect on fracture energy of concrete and stability issues in three-point bending fracture toughness testing*, ACI Mater. J., **92**, 5, 483–496, 1995.
44. R. H. J. PEERLINGS, *Enhanced damage modeling for fracture and fatigue*, PhD Thesis, TU Eindhoven, Eindhoven, 1999.
45. G. PIJAUDIER-CABOT, Z. P. BAŽANT, *Nonlocal damage theory*, ASCE J. Eng. Mech., **113**, 1512–1533, 1987.
46. G. PIJAUDIER-CABOT, K. HAIDAR, J. F. DUBE, *Non-local damage model with evolving internal length*, Int. J. Num. and Anal. Meths. in Geomech., **28**, 633–652, 2004.
47. C. POLIZZOTTO, G. BORINO, P. FUSCHI, *A thermodynamic consistent formulation of nonlocal and gradient plasticity*, Mech. Res. Communic., **25**, 75–82, 1998.
48. H. W. REINHARDT, H. A. W. CORNELISSEN, D. A. HORDIJK, *Tensile tests and failure analysis of concrete*, J. Struct. Engrg. ASCE, **112**, 2462–2477, 1986.
49. S. ROLSHOVEN, *Nonlocal plasticity models for localized failure*, PhD Thesis, École Polytechnique Fédérale de Lausanne, 2003.
50. M. R. SALARI, S. SAEB, K. WILLAM, S. J. PATCHET, R. C. CARRASCO, *A coupled elastoplastic damage model for geomaterials*, Computers Methods in Applied Mechanics and Engineering, **193**, 2625–2643, 2004.
51. J. C. SIMO, J. W. JU, *Strain- and stress-based continuum damage models – I. Formulation*, Int. J. of Solids Structures, **23**, 7, 821–840, 1987.

- 
52. A. SIMONE, *Continuous-discontinuous modelling of failure*, PhD Thesis, Delft University, 2003.
  53. L. SKARŻYŃSKI, E. SYROKA, J. TEJCHMAN, *Measurements and calculations of the width of the fracture process zones on the surface of notched concrete beams*, *Strains*, doi: 10.1111/j.1475-1305.2008.00605.x, 2009.
  54. L. SKARŻYŃSKI, J. TEJCHMAN, *Calculations of fracture process zones on meso-scale in notched concrete beams subjected to three-point bending*, *European Journal of Mechanics/A Solids*, **29**, 746–760, 2010.
  55. A. SIMONE, G. N. WELLS, L. J. SLUYS, *Discontinuous Modelling of Crack Propagation in a Gradient Enhanced Continuum*, Proc. of the Fifth World Congress on Computational Mechanics WCCM V, Vienna, 2002.
  56. L. STRÖMBERG, M. RISTINMAA, *FE-formulation of nonlocal plasticity theory*, *Comput. Methods Appl. Mech. Engrg.*, **136**, 127–144, 1996.
  57. E. SYROKA, J. BOBIŃSKI, J. TEJCHMAN, *FE analysis of reinforced concrete corbels with enhanced continuum models*, *Finite Element Methods in Analysis and Design*, 10.1016/j.finel.2011.03.022, 2001.
  58. E. SYROKA-KOROL, *Experimental and theoretical investigations of size effects in concrete and reinforced concrete beams*, PhD Thesis, Gdańsk University of Technology, 2011.
  59. L. WIDULINSKI, J. TEJCHMAN, J. KOZICKI, D. LEŚNIEWSKA, *Discrete simulations of shear zone patterning in sand in earth pressure problems of a retaining wall*, *Int. J. Solids and Structures*, **48**, 7–8, 1191–1209, 2011.
  60. M. R. A. VAN VLIET, J. G. M. VAN MIER, *Experimental investigation of size effect in concrete and sandstone under uniaxial tension*, *Engineering Fracture Mechanics*, **65**, 165–188, 2000.
  61. G. Z. VOYIADJIS, Z. N. TAQIEDDIN, P. KATTAN, *Theoretical formulation of a coupled elastic-plastic anisotropic damage model for concrete using the strain energy equivalence concept*, *International Journal of Damage Mechanics*, to appear.

Received May 2, 2011; revised version November 4, 2011.

---